Copyright © 2005 IEEE. Reprinted from RADECS Proceedings

This material is posted here with permission of the IEEE. Such permission of the IEEE does not in any way imply IEEE endorsement of any of Jet Propulsion Laboratory's products or services. Internal or personal use of this material is permitted. However, permission to reprint/republish this material for advertising or promotional purposes or for creating new collective works for resale or redistribution must be obtained from the IEEE by writing to pubs-permissions@ieee.org.

By choosing to view this document, you agree to all provisions of the copyright laws protecting it.

Radial Dose Profiles: Calculation Refinements and Sensitivities to Single Event Effects Analysis

Jeffrey Patterson and Randall Swimm
Jet Propulsion Laboratory
California Institute of Technology
Mail Stop 303-220
4800 Oak Grove Drive
Pasadena, California 91109-8099, USA

Abstract: Comparisons of radial dose calculation are performed, as well as the introduction of important physics to improve the calculation techniques. Also, the consequences to device performance are explored via numerical simulations.

I. Introduction

For space missions, single event effect testing is performed utilizing accelerated heavy ion beams to reproduce the linear energy transfer (LET) spectrum of the galactic cosmic ray (GCR) environment. Although similar LETs are achieved, the energies of the accelerated beams are significantly lower than a large fraction of the GCR flux. In fact, the accelerator beams used would be effectively attenuated with nominal amounts of spacecraft shielding, i.e. the majority of cosmic rays that strike the sensitive microelectronic devices in space are significantly more energetic than the ions available for testing purposes. The difference in energy scales has several adverse consequences, which are well documented in the literature. At best, the interpretations of the tests become more problematic, and at worst, the applicability of the results is severely limited.

One complication resulting from this energy difference is the track structure, i.e. although the same amount of charge per unit path length is initially liberated by accelerated beams and cosmic rays, the distribution about the axis of the ion strike is different. Therefore the amount of charge that escapes recombination and ultimately gets collected to upset the performance of the device varies. This can be understood intuitively by considering the energy spectrum of the liberated electrons. The more energetic ions will produce higher energy delta rays, which will result in a more diffuse, wider column of liberated charge, while the less energetic accelerator beam will produce a more concentrated, thinner column of charge. The effect these distributions can have on a particular device can potentially differ.

Much work has been done to quantifying the radial track distribution, and the sensitivity of the dynamics of the charge collection process to the radial distribution of charge. Fageeha el al [1] used Rutherford scattering and delta ray theory to determine the radial dose distribution for an arbitrary ion strike in an arbitrary target material. Kobayashi et al [2] used this formalism to validate GEANT4 Monte Carlo simulations of a 100 MeV incident proton strike on silicon.

One goal of this work is to provide refinements to the radial dose calculations by introducing some physical considerations that are currently left out of the existing formalsim. As will be shown, this will allow for greater agreement with the currently accepted LET values. Another aspect of this work is the investigation of qualitative trends regarding the effect these differing track structures to the final SEE performance of a device. Finite element simulations of charge collection from ion strikes of various radial densities in a semiconductor device are used for this purpose.

II. Radial Dose Calculations

The radial dose profile from an ionizing particle strike in water is calculated by starting with Rutherford scattering to determine the energy distribution of the secondary electrons, and integrating across concentric cylindrical shells to determine the energy flux leaving the shells as a function of radius. Fageeha [1] proposed an extension to arbitrary materials, including silicon. The "material independent" dose, as a function of perpendicular distance from the incident ion's axis, $D_1(t)$, where t is in nm is

The research in this paper was carried out at the Jet Propulsion Laboratory, California Institute of Technology, under contract with the National Aeronautics and Space Administration (NASA).

Authorized licensed use limited to: IEEE Xplore. Downloaded on March 17, 2009 at 13:09 from IEEE Xplore. Restrictions apply.

$$D_1(t) = \frac{Ne^4 Z^{*2}}{\alpha m_e c^2 \beta^2 t}\left[\frac{\left(1-\frac{t+\theta}{T+\theta}\right)^{\frac{1}{\alpha}}}{t+\theta}\right]$$

, (1)

where N is the electron density of the target material ($7*10^{23}$ cm^{-3} for silicon), e is the fundamental electric charge, Z^* is the "effective" charge of the incident particle, calculated via the Barkas formula, m_e is the rest mass of the electron, c is the speed of light in a vacuum, and α is a constant defined below. Because the constant $Ne^4/(m_e c^2)$ shows up in many calculations in this work, the numerical value of for silicon is $2.84*10^{-2}$ MeV-cm^{-1} . θ is the range (in the target material) of a delta ray with kinetic energy equal to the mean excitation energy (3.8 eV in Si), and T is the maximum range of a delta ray. From two body interactions, the maximum energy of a delta ray, W_{max}, is

$$W_{\max} = \frac{2m_e c^2 \beta^2}{1-\beta^2}, \quad (2)$$

$D_1(t)$ is then corrected with an empirical expression to achieve greater agreement with Monte Carlo results for the specific target material. D(t) is the "corrected" result

$$D(t) = D_1(t) \times [1 + k(t)], \quad (3)$$

where for silicon only, k(t) takes the form

$$k(t) = A\beta^B (t - 0.1) Exp[-t/C], \quad (4)$$

where B = 0.215, C=3.127, and A=0 for β<0.0081, A=112β-0.899 for 0.0081<β<0.091, and A=0.674β+9.21 for β>0.091.

The calculation of θ and T require the knowledge of r(ω), the range of an electron, with energy ω, in the target material. In both [1] and [2], the simple power law is assumed,

$$r(\omega) = k \cdot \omega^{\alpha}, \quad (5)$$

where ω is in keV, k is a constant quoted as $6*10^6$ g cm^{-2} $keV^{-\alpha}$, and α = 1.079 for ω<1 keV and α=1.667 for ω>1 keV. This is the same α referred to in equation (1). The range r is in units of g cm^{-2}. One obvious drawback to this method is that this power law applies only to silicon. If one wants to calculate the radial dose, as a function of the material, this particular power law will not apply. Also as will be shown below, the power law is not valid for energy ranges associated with cosmic rays.

One refinement this work provides is the application of a more accurate, material independent methodology to calculate θ and T. Nealy et al [3] has proposed a parameterization for the practical range of electrons based on experimental tests involving several materials and a broad energy range (0.3 keV to 30 MeV):

$$r(\omega) = a_1\left[\left(\frac{1}{a_1}\right)\ln(1+a_2\tau) - \left(\frac{a_3\tau}{1+a_4\tau^{a_5}}\right)\right], \quad (6)$$

where $\tau=\omega/m_e c^2$. The coefficients are given in Table 1

a_1	a_2	a_3	a_4	a_5
b_1-A/Z^{b2}	b_3Z	b_4-b_5*Z	b_6-b_7*Z	b_8/Z^{b9}

Table 1-Constants for electron range calculations where Z is the atomic number of the target material and A is the atomic mass of the target material. The bs are given in Table 2

B1	B2	B3	B4	B5
0.2335	1.209	1.78E-4	0.9891	3.01E-4
B6	B7	B8	B9	
1.468	0.0118	1.232	0.109	

Table 2-Material independent constants for the electron range calculation

The precision of this parameterization has been demonstrated in [3], and agrees very well with experimental measurements in the above quoted energy range.

To consider the differences in energy of the most energetic delta rays associated with accelerator beams and cosmic rays, note that accelerated based SEE tests are performed with beams with energies on the order of 25 MeV/amu, and ions with energies greater than 10 GeV/amu are encountered in a space environment. The maximum delta ray energy of a 25 MeV/amu beam in 55 keV (beta=0.43), while the maximum delta ray energy for a 10 GeV/amu particle is 140 MeV (beta=0.99999). Therefore, the delta rays resulting from the earth based accelerators are all un-relativistic, while a large fraction of the cosmic ray induced electrons are extremely relativistic, and thus for a given LET, the dose distribution will be more diffuse for the high energy cosmic ray.

A comparison of the power law and the Nealy method is shown in Figure 1. The x-axis

Authorized licensed use limited to: IEEE Xplore. Downloaded on March 17, 2009 at 13:09 from IEEE Xplore. Restrictions apply.

refers to the electron energy in eV and the y axis is the electron range in silicon in g-cm^{-2}. The dashed curve shows the power law result, while the continuous curve is the parameterization given in [3]. As can be seen in the figure, the power law starts to significantly over predict the range of delta rays at energies greater than 500 keV. Thus the power law formulation of electron range can be used for liberated electrons produced with accelerator ion beams; however, it is inappropriate for energetic cosmic rays.

An obvious metric to quantify the success of a radial distribution methodology is the integration of a disk of charge to determine the total energy per unit length (or LET) that the model reproduces. This value should be in agreement with the work of Zeigler, now embedded in the accepted TRIM [4] application. This integration is shown in equation (7). LET is determined via TRIM

$$err = \frac{2\pi \int_0^{t_{max}} t * D(t)dt}{LET} \quad (7)$$

Err, as calculated via (7) should be slightly greater than 1.0 because the only energy loss mechanism that the delta ray theory assumes is ionization, and other mechanisms such as the interaction with the lattice nuclei are ignored. These processes are included in the TRIM models. The calculated LET values associated with the power law formulation, as well as the Nealy methodology and TRIM, are shown in Tables 3 and 4. Tables 3 shows 3 beams typically used for SEE testing, which are 40 MeV/amu Ne-20, Ar-40, and Kr-78. Table 4 shows the same ions, however, each with the total a total energy of 10 GeV, which is more realistic for the cosmic rays that reach the microelectronic devices in space. All LET values are given in MeV-cm^2/mg.

40 MeV/amu	Ne-20	Ar-40	Kr-78
LET (TRIM)	1.17	3.88	14.61
Err(Power)	1.21	1.17	1.16
Err(Param)	1.16	1.13	1.12

Table 3-Err as calculated via (7) for typical accelerator beams

10 GeV	Ne-20	Ar-40	Kr-78
LET(TRIM)	0.22	1.06	6.56
Err(Power)	1.13	1.09	1.16
Err(Param)	1.08	1.05	1.12

Table 4-Err as calculated via (8) for the ion species in Table 3, however with energies more comparable to those found in the GCR spectrum

We see from Tables 3 and 4, that the use of the parameterized range of electrons improves the accuracy of radial dose calculations from the power law in every instance. Thus the incorporation of a more accurate method of calculating the range of electrons makes an observable increase in the accuracy of charge distribution LET calculations.

To show the discrepancies of the track structures of accelerator beams to GCR, we compare a 40 MeV/amu Ne-20 beam, which has an LET of 1.17 MeV-cm^2/mg to a 10 GeV Ar-40 ion, which has a fairly equivalent LET of 1.15 MeV-cm^2/mg, both values obtained from TRIM. The radial dose profile is shown in Figure 2. What is shown is the percent of total charge contained within a disk of radius t, the x axis in nm. The dashed curve is the lower energy neon beam, while the solid curve represents the high energy argon beam. For the neon beam, 95% of the liberated charge is contained within a radius of approximately 40 nm, while the argon beam is much more diffuse, with 95% of the liberated charged contained in a disk of approximately 200 nm. Note the total amount of charge for both ions is approximately the same; however, the charge for the high energy beam is much more diffuse.

Currently, with state of the art semiconductor foundries at the 90 nm feature size, this result has important implications for the applicability of accelerator based SEE testing. With an accelerator beam, the resulting charge is very concentrated, and the cosmic ray less so. In this way, accelerator testing has the potential to underestimate the threshold LET for single event mechanisms. This implies the ground based SEE testing can be conservative in one respect. However, a more "spread out" cosmic ray can effectively strike more structures, accelerator testing can also underestimate multiple-bit effects, and thus it can also be non-conservative. The consequences for device operation and the physics of charge collection is the topic of the next section.

III. Charge Collection Physics

The above analysis only predicts the immediate (t=0 s) distribution of liberated charge carriers, and does not say anything regarding how the diffusion, drift, and recombination

Authorized licensed use limited to: IEEE Xplore. Downloaded on March 17, 2009 at 13:09 from IEEE Xplore. Restrictions apply.

processes affect the distribution of free charge a short time after the initial ion strike. Immediately, drift and diffusion starts to drive the carriers away from this initial condition, while recombination will eliminate charge from the distribution.

For the more concentrated distributions (accelerator beams), recombination will be more effective in eliminating the initial charge, making the "effective" deposited charge of an accelerator beam somewhat less than that of a cosmic ray of equivalent LET. However, from the greater charge concentration, the diffusion process will also be stronger, and will tend to drive the initial concentration to resemble the more diffuse, cosmic ray concentration, on short time scales, perhaps very short compared to the time required for the majority of the charge to be collected at the reverse biased nodes in the vicinity of the ion strike. We decided that instead of pursuing the complicated closed form analytic techniques to investigate these numerous competing effects, the more efficient tool would be one of the commercially available device simulation packages that already contain robust physics models, as well as powerful numerical techniques required to approximate solutions to the mixed boundary value problems that arise when studying the flow of free carriers in semiconductor devices.

IV. Charge Collection Simulations

To investigate the effects of varying the track width on charge collection physics, we employed the Synopsys TCAD package, GENESIS. A two dimensional "virtual" device was used to study how the track width influenced the amount of charge collected at various nodes. The device consisted of 21 identical diodes, with highly doped (10^{19} particles/cm^3) p wells arranged in a collinear fashion, and all sharing a common lightly doped ($5*10^{15}$ particles/cm^3) n body. Each well has an individual polysilicon contact but share a common body contact, so that the bias for each diode can be independently varied. The width of each well is 100 nm, and the center-center distance between the wells is 200 nm. The depth of each well is 40 nm. The width and depth of the body is 4.3 μm and 20 μm respectively. Although the doping and geometry does not exactly match 90 nm foundries, these values were chosen to approximate the trends that would be observed in an actual device produced in current industry foundries. The diodes were numbered sequentially 1 to 21, with diode 11 being located at the center of the device. See Figure 3. Note the vertical line of symmetry thru diode 11. In order to verify the electrical operation of the device, the I-V curve for each diode was simulated, with the expected results.

The goal of this work is to investigate the qualitative effects of varying the radial distribution of ionization and to discover trends in the total amount of charge collected at reverse biased nodes at varying distances from the center of the ion strike. To achieve this, a vertical track of ionization was placed at the center diode (x = 0 μm) running through the entire height of the device. For this work, a constant LET of 48.3 MeV cm^2/mg was used to produce enough free carriers to obtain significant amount of charge collected at the nodes. The simulation software defines the lateral ionization distribution as a Gaussian. As seen above in section II, the radial distribution is not as simple as a Gaussian. However, we believe that for the investigation of qualitative trends, the approximation of a Gaussian is appropriate. See Figure 4.

A simulation run is defined as a 2D dynamic simulation that begins with all 21 nodes reversed biased at 5 V at t=0 s. At $t=1*10^{-11}$ s, an ion strike is simulated by the production of the vertical ionization track, with a particular value of σ_c which is the sigma associated with the radial charge distribution. A slightly unphysical aspect of the simulation is that production of the ionization charge is Gaussian in time, with an associated $\sigma_t = 2*10^{-12}$ s. Thus for these simulations, the peak rate of ionization production occurs at $t=1*10^{11}$ s, however charge starts being produced before that according to the Gaussian distribution. One can observe this while looking at the transients produced on the output nodes. See Figure 5. The free charge is collected at the various reverse biased nodes via the drift and diffusion processes, which produces current transients of varying amplitude and duration. The simulation is carried out until all transients die out and each diode returns to its initial small leakage current, which takes on the order of 1 μs.

Figure 5 shows a plot of both the instantaneous current and total charge deposited at nodes 1 through 11 (due to the symmetry of the device, nodes 12-21 are not shown), as a function of time. For this simulation, the ion strike has a σ_c of 0.5 μm. Due to the large number of curves, a plot key is not shown; however the data is consistent with physical intuition. The x axis is in units of seconds while

Authorized licensed use limited to: IEEE Xplore. Downloaded on March 17, 2009 at 13:09 from IEEE Xplore. Restrictions apply.

left y- axis refers to current in amps and the right y-axis refers to total collected charge in coulombs. The family of 11 transient curves (one for each node) starting to appear shortly after $t = 1*10^{-11}$ s, while the time integral of these curves are the collected charge and are the other set of curves. The largest (most negative) of the transient curves (black-hashed) in the one associated with diode 11, while each successive curve corresponds to one node over, with the smallest one (black-solid) associated with diode 1. Likewise, the charge collected at node 11 as a function of time is represented by the most negative curve and the charge collected at node 1 is shown in the least negative curve, with the successive curves lying in between. The negative nature of the curves is due to an artifact of the simulation software. The convention of the application is to consider flow of electrons to produce a positive current. The transient current is dominated by holes and thus produces a negative current. Since the collected charge is the time integral of the current, a negative sign appears there also. The interpretation of the data is straight forward. The node closest to the ion strike collects the most charge and the node farthest away collects the least. Note that for the nodes far away from the strike, at times initially after the strike, the current is positive, and at those times, is dominated by electron flow.

V. Simulation Results

For this study, we varied σ_e with values of 0.01, 0.1, 0.25, 0.50, 0.75, 1.00, and 1.50 μm. These values are somewhat arbitrary and the larger values are extreme in that only the most energetic of cosmic rays, which are very rare, would have an ionization track this diffuse. However, since we are trying to observe trends, we felt justified in using this range of values. The results are summarized in Figure 6.

Figure 6 shows the total charge collected at nodes 3 thru 11 for the 7 σ_e values, all with an LET of 48.3 MeV cm^2/mg. Note that nodes 1 and 2 are left off because of the proximity to the unnatural edge boundary, which influenced the charge collected in this region. The data points for the σ_e values of 0.01, 0.50, 1.00, and 1.50 μm have been connected in order to provide more clarity of the trends displayed. The simulations are consistent with the physical intuition detailed in section III. Looking at the data points associated with the most concentrated track, i.e. $\sigma_e = 0.01$ (the dark blue diamonds), it is apparent that the inner nodes collect more charge than any of the more diffuse beams, but the out nodes collect the least amount of charge. Similarly, the most diffuse beam, i.e $\sigma_e = 1.5$ (the light blue + signs) the charge is more evenly distributed across the available nodes, but each one collects less charge than the central ones in the more dense scenarios. Thus the more dense tracks (or less energetic ions) result in a charge collection response that is strongly dependant on the location of the ion strike relative to the collection node. Conversely, the more diffuse tracks (or more energetic ions) result in a more uniform charge collection response across collection nodes at various distances from ion strike.

As foundry feature sizes continue to shrink and the aerial density of sensitive targets continue to increase, the effect of ion energy will become more significant. As the feature sizes decrease, the characterization of SEE response of digital devices as a function of LET only will not be adequate, and the inclusion of energy dependencies will also need to be accounted for in a typical SEE analysis.

VI. Future Work and Limitations of the Simulations

Some discussion on the limitations of the 2D simulations is appropriate. In any finite element analysis, such as these simulations, there is always a tradeoff between accuracy and computation time. For the device level simulations, a meshing grid is imposed on the system of study, with finer grids resulting in more accurate solutions, but with increased computation time. In order to have confidence in simulation studies, one must understand the stability of the solutions as a function of the grid imposed on the system. One of the more difficult aspects of this work is providing enough resolution in the grid over regions where the doping, internal electric fields, and charge flow densities are great, but not over specifying the grid in regions where these densities are not as great. The results presented here are performed with a meshing containing approximately 9000 grid points. Doubling that number leads to a significant increase in the time required to perform the simulations, and changes the results on the order of 2%. There is an inherent error bar in this work associated with the imposed grid, however because currently we are investigating general trends, this is acceptable.

Another approximation employed in this work is the geometry of the device. In any

Authorized licensed use limited to: IEEE Xplore. Downloaded on March 17, 2009 at 13:09 from IEEE Xplore. Restrictions apply.

real device, the upper surface would have a layer of isolating oxide between the separate contacts. The simulations performed here do not have such an oxide present. We have performed some preliminary simulations with an insulator placed there. Our initial results show that the overall current in each node is not strongly dependant on the presence of such a layer. However, in these preliminary simulations some subtle differences in current densities throughout the bulk of the device appear, of which we are still studying the results.

This work also uses a fairly deep charge collection depth of 20 μm, i.e. the ionization track extends the entire depth of the device. The distance charge deposited near x = 0 μm, y = 20 μm has to travel to reach node 1 does not significantly differ from that to reach node 11. We have also performed preliminary simulations where the ion stops 5 μm into the body to mimic devices which have truncated charge collection volumes such as SOI or epi technologies. This scenario produces a much stronger dependence of the charge collected at the various nodes, and thus the results presented here underestimate the trends for devices with shallow charge collection volumes. However, the results are still very preliminary, and thus fall under to topic of future work.

VII. Conclusions

The first part of this work integrated a more accurate relationship between the range and energy of electrons in any given atomic material into the delta ray theory that is currently used to calculate the radial charge distribution resulting from energetic ion strikes. It was shown that the inclusion of this parameterization results in LET values more consistent with the widely accepted TRIM results than those using the standard power law for range in silicon only. Using these calculations, this section also demonstrated the differences in the radial charge distribution from an extremely energetic ion strike (similar to those in the GCR spectrum) and an ion strike with a similar LET but with a lower energy, comparable to accelerator beams used in typical SEE testing.

To understand the qualitative differences this discrepancy can potentially introduce in testing results, in the second section of this work device level simulations were performed. Charge collection experiments were performed on a virtual device by varying the width of a Gaussian ion strike, and observing the resulting differences in the transients at reverse biased diodes at various distances from the center of the charge distribution function. The different widths of the initial charge distribution would correspond to ion hits of varying energy, but constant LET. A summary of these simulations is shown in Figure 6.

The more dense distributions result in more charge being collected at nodes near the strike, but less charge at the distant nodes. The more diffuse beams result in a more uniform quantity of charge being deposited at each node, but with less total charge than the inner nodes of the dense beams. These trends are in agreement with physical intuition, and thus the outputs of these simulations are confirmed to be consistent with the general trends of a real charge collection experiment. However, the limitations of this work are documented in section VI, and these results should only be taken as qualitative trends. We are refining our simulations and will publish quantitative results in a later work.

These observed trends do verify that as the feature size of digital electronics decrease, the discrepancy in energy of galactic cosmic rays and the ions the community uses to perform SEE testing will result in erroneous testing results. Namely, the accelerator beams will overestimate the cross sections for single node upsets, but can potentially underestimate the multiple node effects, that will occur due to the more radially diffuse extremely energetic cosmic rays.

References

[1] O. Fageeha, J. Howard, and R. C. Block, "Distribution of radial energy deposition around the track of energetic particles in silicon", J. Appl. Phys. 75 (5), March 1994, p. 2317-2321

[2] A. Kobayashi, A. Sternberg, L. Massengill, R. Shrimpf, and R. Weller, "Spatial and Temporal Characteristics of Energy Deposition by Protons and Alpha Particles in Silicon", IEEE Trans. Nucl. Sci., Vol 51, No 6, December 20004, p. 3312-3317

[3] Nealy, et al, "Transport of Space Environment Electrons: A Simplified Rapid Analysis Computational Procedure", NASA/TP-2002-211448, March 2002

[4] www.srimm.org

[5] Cucinotta et al, "Heavy Ion Track Structure Calculations for Radial Dose in Arbitrary Material", NASA Technical Memorandum 3497, Feb 1995

Authorized licensed use limited to: IEEE Xplore. Downloaded on March 17, 2009 at 13:09 from IEEE Xplore. Restrictions apply.

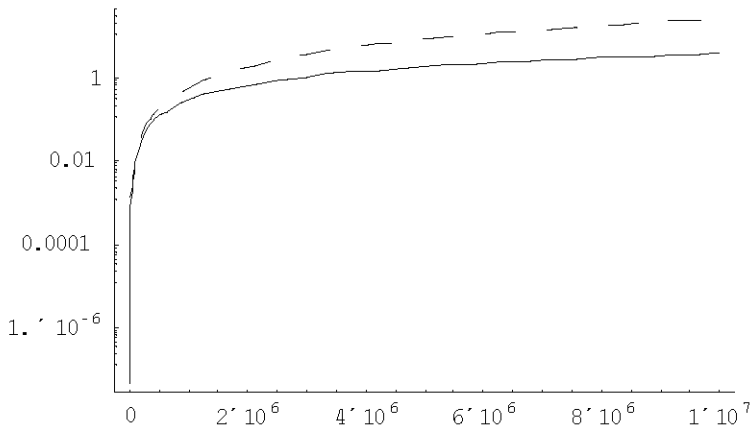

Figure 1 – Comparison of the power law and Nealy methodologies to determine the range of delta rays in silicon as a function of kinetic energy (in eV)

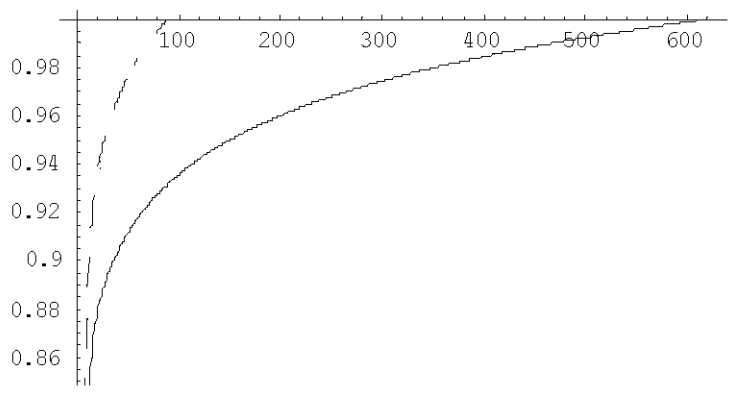

Figure 2 – Faction of total charge liberated in a disk of radius t (in nm). The dashed curve is a 40 MeV/amu Ne-20 beam while the continuous curve is a 10 GeV Ar-40 beam.

Authorized licensed use limited to: IEEE Xplore. Downloaded on March 17, 2009 at 13:09 from IEEE Xplore. Restrictions apply.

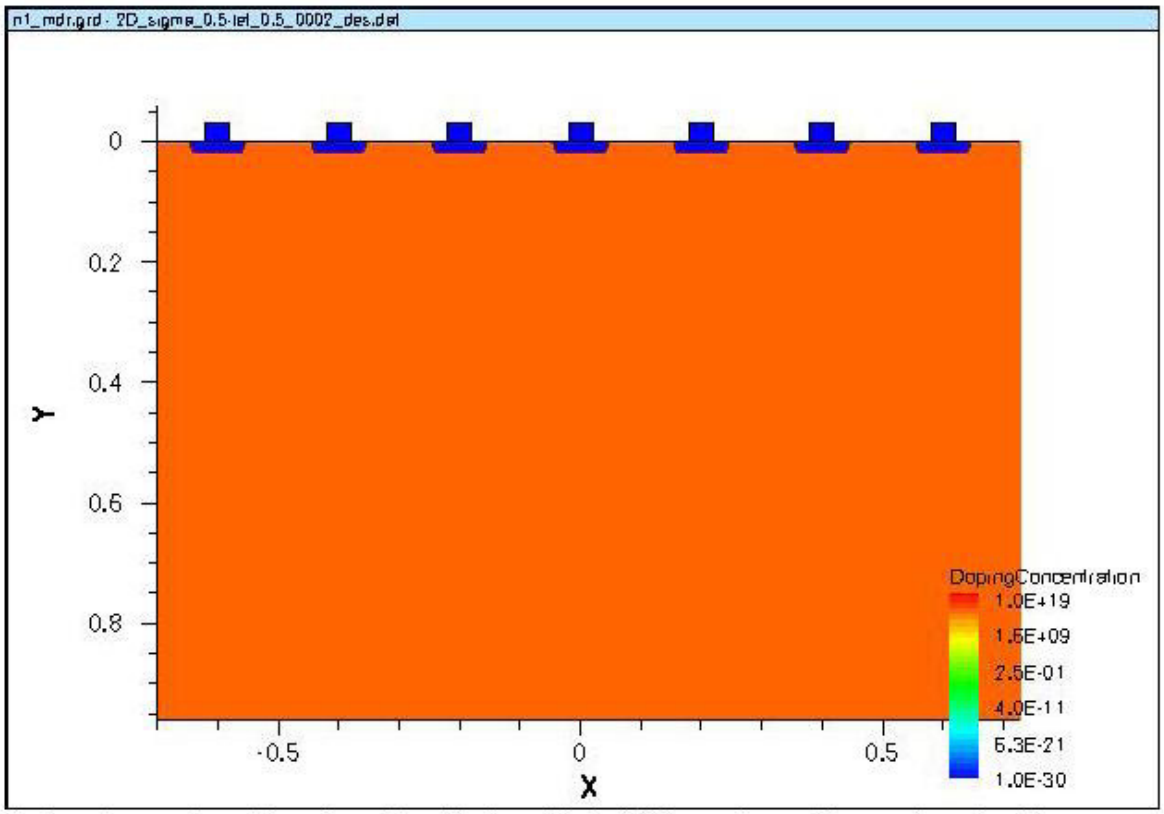

Figure 3 – A cut away of a portion of our virtual device. Diodes 8 -14 are shown. The x and y axis units are µm. Note, diode 11 is centered at x=0. The device extends in the x axis -2.15 to 2.15 µm, for all 21 diodes and in the y direction to y=20 µm. The blue (p type) wells are doped with boron to a level of 10^{19} particles/cm^3 and the orange (n type) with arsenic to a level of $5*10^{15}$ particles/cm^3. Note the blue polysilicon rectangular contacts on top of each well.

Authorized licensed use limited to: IEEE Xplore. Downloaded on March 17, 2009 at 13:09 from IEEE Xplore. Restrictions apply.

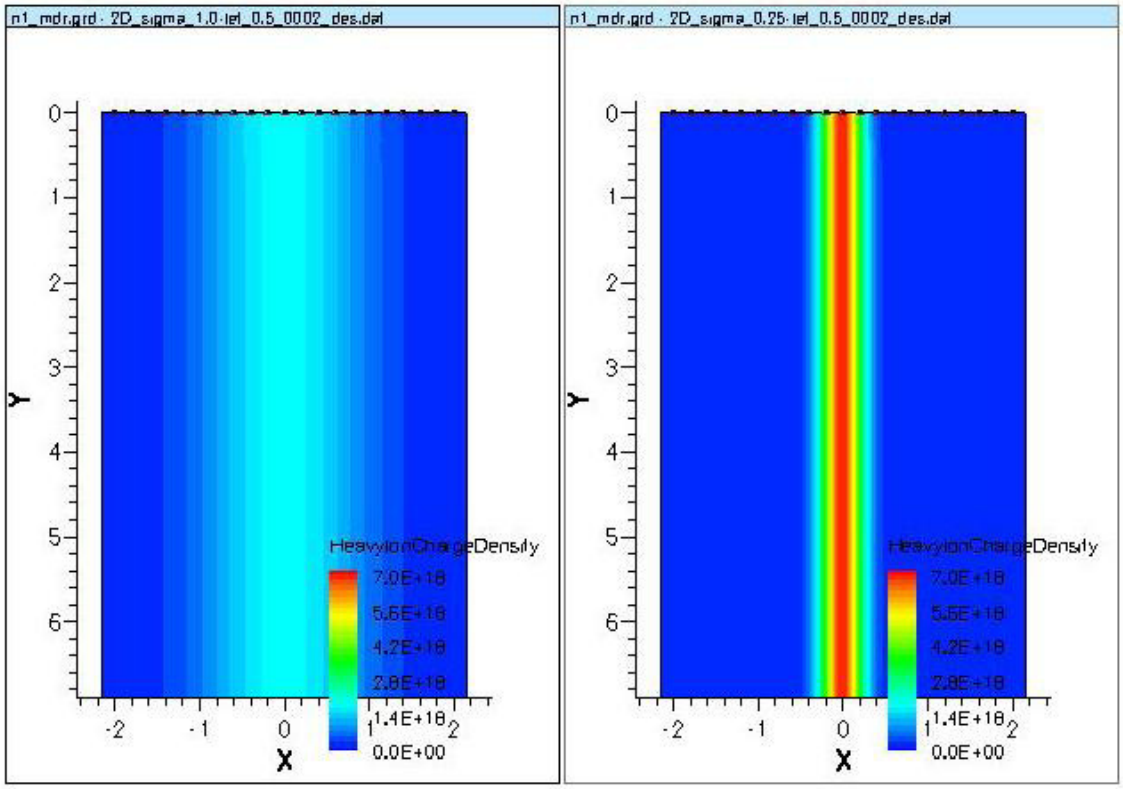

(a) **(b)**

Figure 4 – Ion strikes in the virtual charge collection device. Charge density plots for two ion strikes with the same LET (48.3 MeV cm^2/mg), but with different radial sigma (a) $\sigma = 1.0$ µm (b) $\sigma = 0.25$ µm. Note each distribution contains the same charge per unit length; however (a) is much more radially diffuse than (b). Each track will affect multiple diodes.

Authorized licensed use limited to: IEEE Xplore. Downloaded on March 17, 2009 at 13:09 from IEEE Xplore. Restrictions apply.

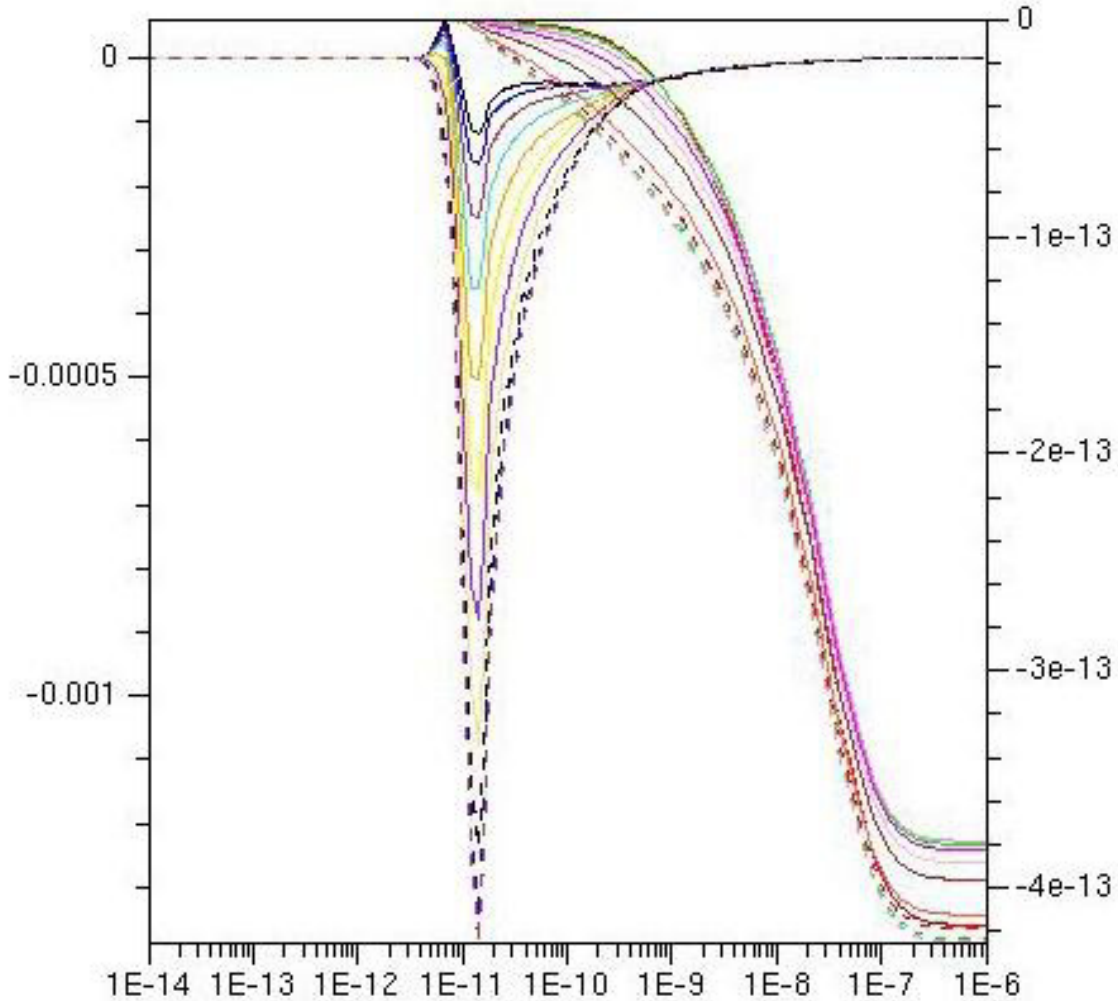

Figure 5 – The instantaneous current and total collected charge at nodes 1 thru 11 from an ion strike at t = $1*10^{-11}$ s, with an LET of 48.3 MeV cm^2/mg and a σ_e = 0.5. The x axis is in units of seconds while left y-axis refers to current in units of A and the right y-axis refers to total collected charge in units of C. The family of 11 transient curves (one for each node) starting to appear shortly after t = $1*10^{-11}$ s, while the time integral of these curves are the collected charge and are the other set of curves.

Authorized licensed use limited to: IEEE Xplore. Downloaded on March 17, 2009 at 13:09 from IEEE Xplore. Restrictions apply.

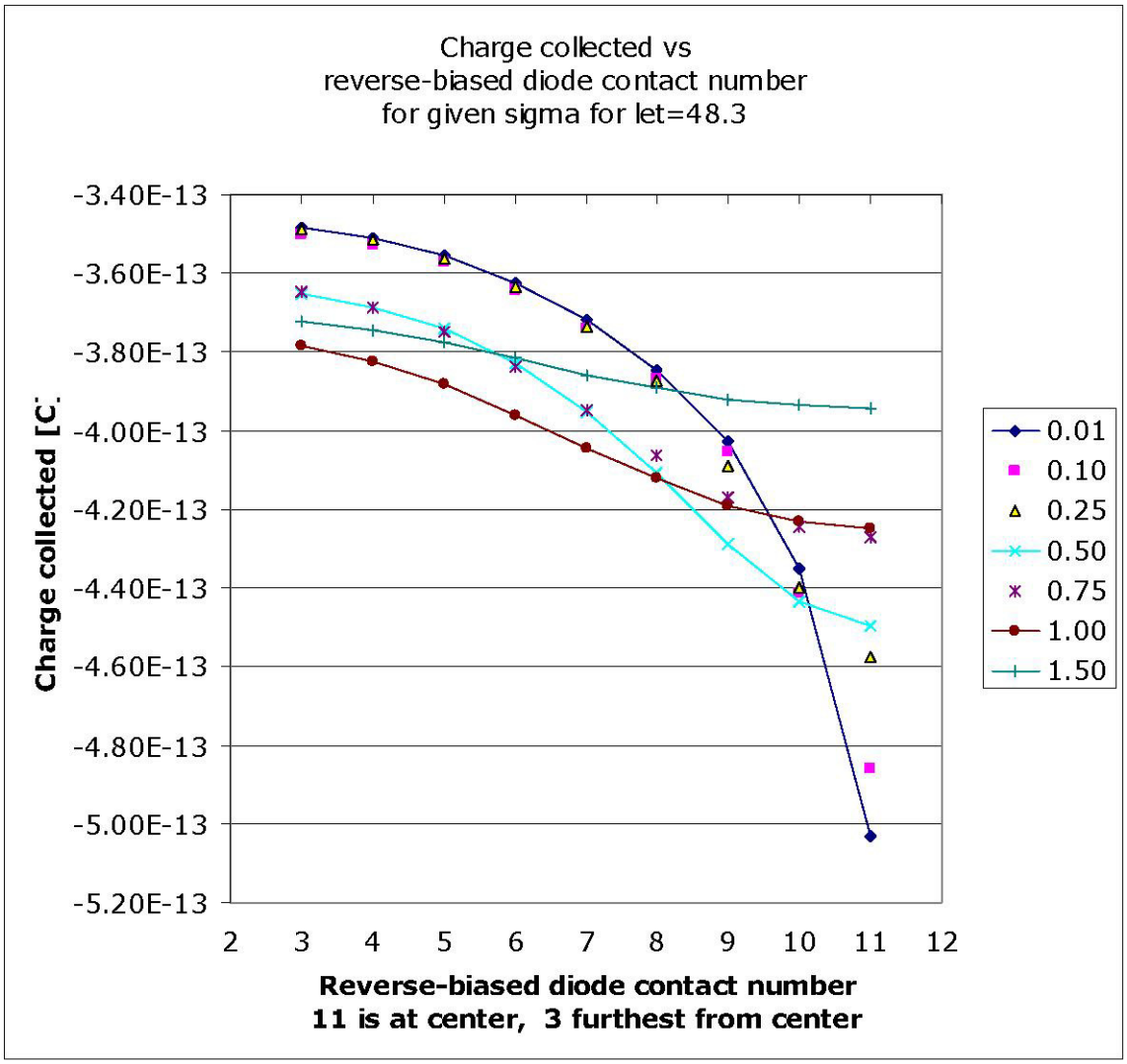

Figure 6 – The total charge collected at nodes 3 thru 11 for the seven σ_e values used in this study. The data points for σ_e = 0.01, 0.50, 1.00, and 1.50 μm have been connected with curves in order to more easily observe the charge collection trends.

Authorized licensed use limited to: IEEE Xplore. Downloaded on March 17, 2009 at 13:09 from IEEE Xplore. Restrictions apply.